Optical absorption and photoluminescence of ZnSe microcrystals in a Pyrex glass matrix

1996 J. Phys.: Condens. Matter 8 7509

(http://iopscience.iop.org/0953-8984/8/40/014)

J. Phys.: Condens. Matter **8** (1996) 7509–7521. Printed in the UK

Optical absorption and photoluminescence of ZnSe microcrystals in a Pyrex glass matrix

Shosuke Mochizuki and Kouta Umezawa

Department of Physics, College of Humanities and Sciences, Nihon University, 3-25-40 Sakurajosui, Setagaya-ku, Tokyo 156, Japan

Received 4 March 1996, in final form 15 July 1996

Abstract. ZnSe microcrystals have been embedded into Pyrex glass matrix for the first time. The optical extinction and photoluminescence spectra of these ZnSe-doped (-embedded) glasses are measured at various temperatures. The specimens exhibit a clear shift of the optical extinction (absorption) edge due to the spatial confinement of carriers and excitons in three dimensions. Also, the photoluminescence spectra show a weak edge emission band at their absorption edges and an intense broad emission band at longer wavelength. The broad emission band shifts to the longer-wavelength side with increasing time elapsed after excitation. Taking into account some imperfections in the crystallite and impurities in the matrix glass, the results obtained are discussed and are compared with the properties of ZnSe bulk and film crystals.

1. Introduction

The optical properties of semiconductor microcrystals provide information on the three-dimensional confinement of carriers (electrons and holes) and of excitons by a deep surface potential well and on the surface electronic states. For such confinement, two kinds of confinement effect are suggested theoretically. On decreasing the crystallite size, the effect of quantization on exciton motion becomes prominent. When the crystallite's size decreases further to the exciton Bohr radius, the character of excitons disappears, and the electron and hole become individually confined (Efros and Efros 1982). On the other hand, there are some fundamental problems as regards the electronic states at the crystallite surface. For example, the details of exciton and carrier dynamics at the crystallite's surface are of great interest as regards the persistent hole-burning and photo-darkening effects. In recent years, the optical spectra of CuCl, CuBr, CdS, CdSe, CdS_xSe_{1-x}, Ge and Si microcrystals embedded in glass, liquid and polymer matrices have been investigated extensively.

In the present paper, we report in detail the optical spectra of ZnSe microcrystals embedded into Pyrex glass (ZnSe-doped glass). Bulk ZnSe crystal is a well-characterized semiconductor with a wide direct band gap near 2.72 eV at room temperature and is known also as a candidate material for blue-colour-laser material. However, the reports on the optical properties of ZnSe microcrystals are limited in number. Brus (1986) and Chestnoy *et al* (1986) have already reported preliminary results on the optical extinction spectra of ZnSe microcrystals in liquid.

0953-8984/96/407509+13$19.50

2. Experimental details

2.1. Specimen preparation

Embedded ZnSe microcrystal specimens were prepared as follows. We heated Pyrex glass (Na_2O–B_2O_3–SiO_2) at about 1573 K for a day and then we put nominally pure ZnSe bulk crystal into the molten glass. The volume fraction of ZnSe was 0.006. After two days, the molten glass containing ZnSe was cooled rapidly to room temperature to suppress the nucleation of ZnSe microcrystals. The glass obtained was transparent. The glass was then annealed at 973 K in air for the desired time to grow ZnSe microcrystals. It has been deduced theoretically that the average radius R of microcrystals grown in a matrix should increase with the one-third power of the heat treatment time (Lifshitz and Slezov 1958).

2.2. Optical measurements

The transmission and photoluminescence measurements on the ZnSe-doped glass were performed at various temperatures from 7 K to room temperature as a function of heat treatment time. The transmitted and emitted lights were dispersed using a grating spectrograph (Jobin–Yvon HR-320), and a multichannel photo-detection system is employed. Since the transmission spectra T_r obtained contain the effects of both scattering and absorption, the results are expressed as extinction spectra, $-\log T_r$. The photoluminescence spectra observed were corrected for the spectral response of the measurement system.

3. Results and discussion

3.1. Optical spectra at room temperature

Figure 1 shows the extinction spectra of ZnSe-doped Pyrex glass heat treated for different times. The measurements were made at room temperature. No absorption and no emission characteristic of ZnSe were observed in the virgin glass 1. After ten minutes' heat treatment, the weak absorption due to ZnSe appears and grows. With further progressing heat treatment, a shoulder (terrace) structure characteristic of ZnSe becomes prominent and then shifts toward the absorption edge energy of bulk ZnSe crystal. The edge observed at the early stage of heat treatment is blue-shifted considerably from the bulk value (about 456.7 nm = 2.715 eV) at room temperature. Chestnoy *et al* (1986) have reported the molecular orbital diagram with a HOMO–LUMO gap (edge value) of 3.58 eV for a microcrystal 4.4 nm in size. The theoretical gap value is larger than that obtained in the present experiments. The sharp structure at 465 nm is not necessarily reproduced for different specimens, though the wavelength corresponds to the band gap of ZnSe bulk crystal.

Figure 2(a) shows the photoluminescence spectra of ZnSe-doped Pyrex glass heat treated for different times. The measurements were carried out at room temperature under 337.1 nm nitrogen-laser-light excitation. In spectra 1 and 2, the weak emission band at about 390 nm is due to Pyrex glass, and intense longer-wavelength emissions at about 500 nm are due to ZnSe microcrystals. With increasing heat treatment time, a weak emission band grows at the extinction edge and the intense broad emission band shifts to longer wavelength as seen from spectra 3 and 4. Similar spectra have been observed for CdSe (Borrelli *et al* 1987) and CdS_xSe_{1-x} microcrystals (Warnock and Awschalom 1985). The emission observed near the extinction edge was assigned to exciton recombination, while the emission band observed at long wavelength was assigned to surface-related defects. In any case, in the

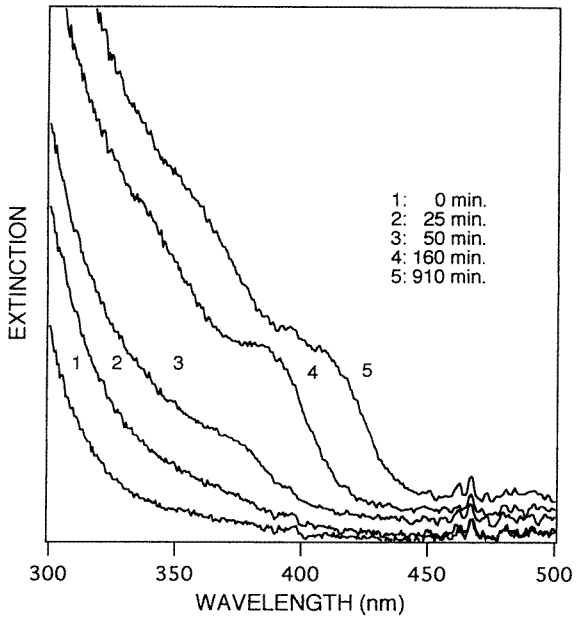

Figure 1. Extinction spectra of ZnSe-doped Pyrex glass heat treated for different times.

present paper, we call the emission observed at the extinction edge 'edge emission' and the emission at long wavelength 'deep-level (DP) emission'. The deep-level emission will be discussed in later paragraphs and sections on the basis of a comparison of the spectra with those observed for bulk and film specimens.

Also, we have made measurements for nominally pure ZnSe bulk crystal that was a piece of the starting material for the ZnSe-doped glass. The spectra obtained at 8 K and 294 K are shown in figure 2(b). An intense sharp high-energy band and very weak low-energy bands are observed at 8 K. The former is predominantly due to the radiative decay of excitons trapped at some defects and impurities, while the latter were similar to those observed for nominally pure thick ZnSe film specimens and were assigned to crystalline defects and impurities (Skromme *et al* 1989, Mohapatra *et al* 1988). With increasing temperature, the weak low-energy bands diminish in intensity and only the intense exciton band is observed at room temperature as shown in figure 2(b).

Incidentally, since we have no direct method of strictly determining the transition energy from the extinction spectra obtained and shown in figure 1 at present, we merely read the terrace edge energy and extinction edge energy. The terrace edge was determined by finding the wavelength at which a tangent on one side of the shoulder intersects with one on the other side. The extinction edge was determined by finding the wavelength at which the tangent on the long-wavelength side of the shoulder intersects the minimum-extinction baseline determined from the long-wavelength region (470 nm $< \lambda <$ 800 nm) of each spectrum. Figure 3 shows the full logarithmic plots of the terrace (shoulder) edge, extinction edge and deep-level emission peak energies against (heat treatment time: $t_H)^{-2/3}$ for three different specimens. The plots indicate some continuous change of slope. Theoretically, if the crystallite structure, composition and shape do not change over the entire size region, such a plot should be a straight line, since the confinement energies of carriers and excitons in

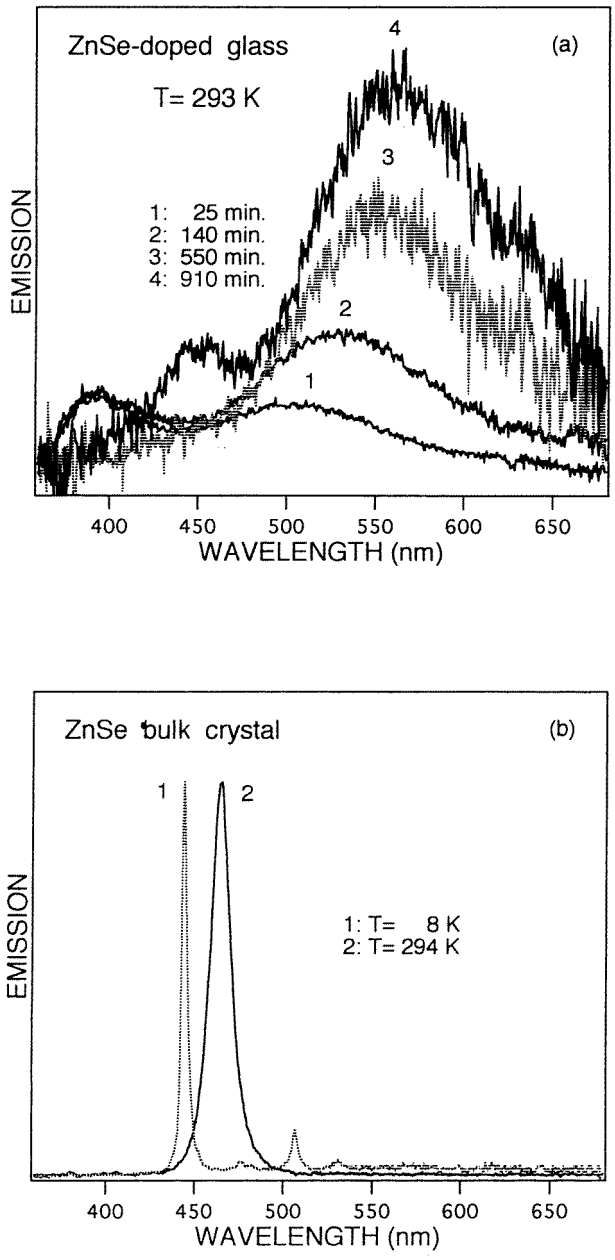

Figure 2. (a) Photoluminescence spectra of ZnSe-doped Pyrex glass heat treated for different times. (b) Photoluminescence spectra of bulk ZnSe crystal.

a sphere of radius R are proportional simply to R^{-2}, and R is proportional to $t_H^{1/3}$. The observed continuous change of the slope may arise from the nature characteristic of small crystallites embedded into matrices. In other word, smaller crystallites may be different from larger crystallites in crystallite structure and shape, or composition.

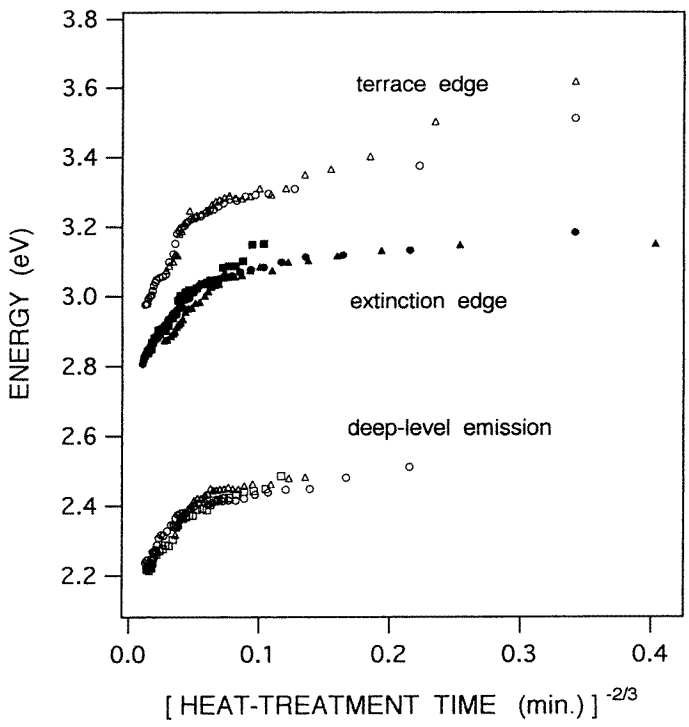

Figure 3. The heat treatment time dependence of the terrace (shoulder) edge, extinction edge and deep-level emission peak energies for three different ZnSe-doped Pyrex glass specimens (circles, triangles and squares).

The observed deviation from the $t_H^{-2/3}$-dependence is also explained by taking into account some surface charge localized at the crystallite–matrix interface. The localized charge may give an additional Coulomb repulsion term, proportional to $1/R$, to the carrier and exciton confinement potentials for smaller crystallites.

Unfortunately, except for for the specimen annealed for 910 minutes, the image resolution of embedded crystallites was not satisfactory in our TEM observation and therefore we estimate tentatively the average crystallite size as follows. The lowest excitation energies E of a spherical crystallite for the carrier and exciton confinements are estimated via the following equations (Brus 1984, Kayanuma 1988): for carrier confinement:

$$E = E_g + (h^2/8R^2)[(1/m_e) + (1/m_h)] - 1.786e^2/\varepsilon R + (\text{polarization term}) \tag{1a}$$

and for exciton confinement:

$$E = E_g - E_b + h^2/[8(m_e + m_h)(R - \eta a_B)^2] \tag{1b}$$

where $E_g, R, \varepsilon, m_e, m_h, E_b$ and a_B are the bulk energy gap, crystallite radius, dielectric constant, electron effective mass, hole effective mass, binding energy of the exciton and Bohr radius of the exciton, respectively. ηa_B is the effective thickness of the exciton dead layer: $0 < \eta < 1$. In the calculation, the following values were used:

$E_g = 2.715$ eV $\quad \varepsilon = 5.75 \quad m_e = 0.16m_0 \quad m_h = 0.75m_0$

$m_0 =$ bare electron mass $\quad a_B = 3.5$ nm $\quad E_b = 0.021$ eV $\quad \eta = 1$ and 0.

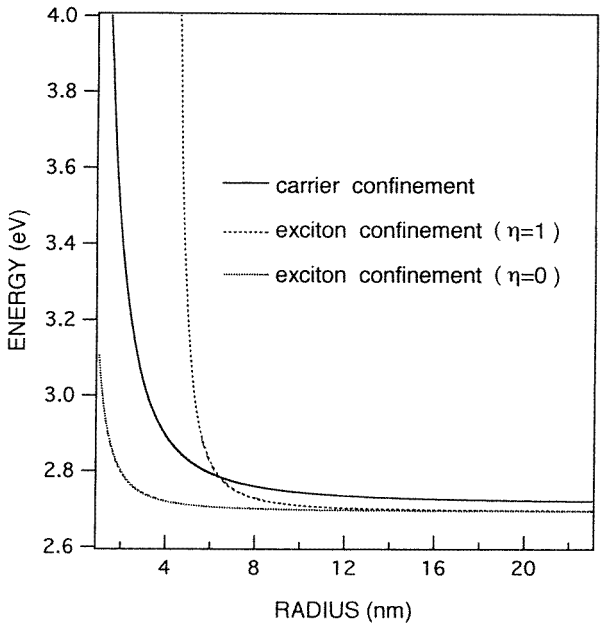

Figure 4. The calculated size dependence of the lowest excitation energies of a ZnSe sphere for the carrier and exciton confinement cases.

The results are shown in figure 4. The calculation for the carrier confinement indicates that the crystallite sizes at the initial and final stages of heat treatment are 2 nm and 20 nm, respectively. The measured average size of ZnSe microcrystals in the glass annealed for 910 minutes was about 22 nm.

3.2. Optical spectra at low temperatures

Figures 5(a) and 5(b) show the extinction and photoluminescence spectra of the specimen heat treated at 973 K for 910 minutes. The extinction spectra are shifted vertically with respect to each other to allow the temperature shift to be seen easily. With decreasing temperature, the extinction edge becomes sharp and shifts to shorter wavelength as shown in figure 6(a). The temperature coefficients of the terrace edge and extinction edge energies for each nearly linear part of the curves at high temperatures are -4.12×10^{-4} eV K^{-1} and -4.08×10^{-4} eV K^{-1}, respectively. Also, with decreasing temperature, the edge emission and deep-level emission bands become sharp and intense, and shift to longer wavelength as shown in figure 6(b). Their temperature coefficients for each nearly linear part of the curves at high temperatures are -4.22×10^{-4} eV K^{-1} and -4.28×10^{-4} eV K^{-1}, respectively. These linear-part values are close to -5×10^{-4} eV K^{-1} which was the linear-part temperature coefficient of the photoluminescence peak energy observed for the same ZnSe bulk crystal as the starting material for the microcrystal specimens. This may indicate that the observed optical properties of the embedded specimens can be explained as a quantum confinement effect of carriers in ZnSe.

Figures 7(a) and 7(b) show the temperature dependences of the edge and deep-level emission intensities of the specimen annealed for 910 minutes. The variation of intensity

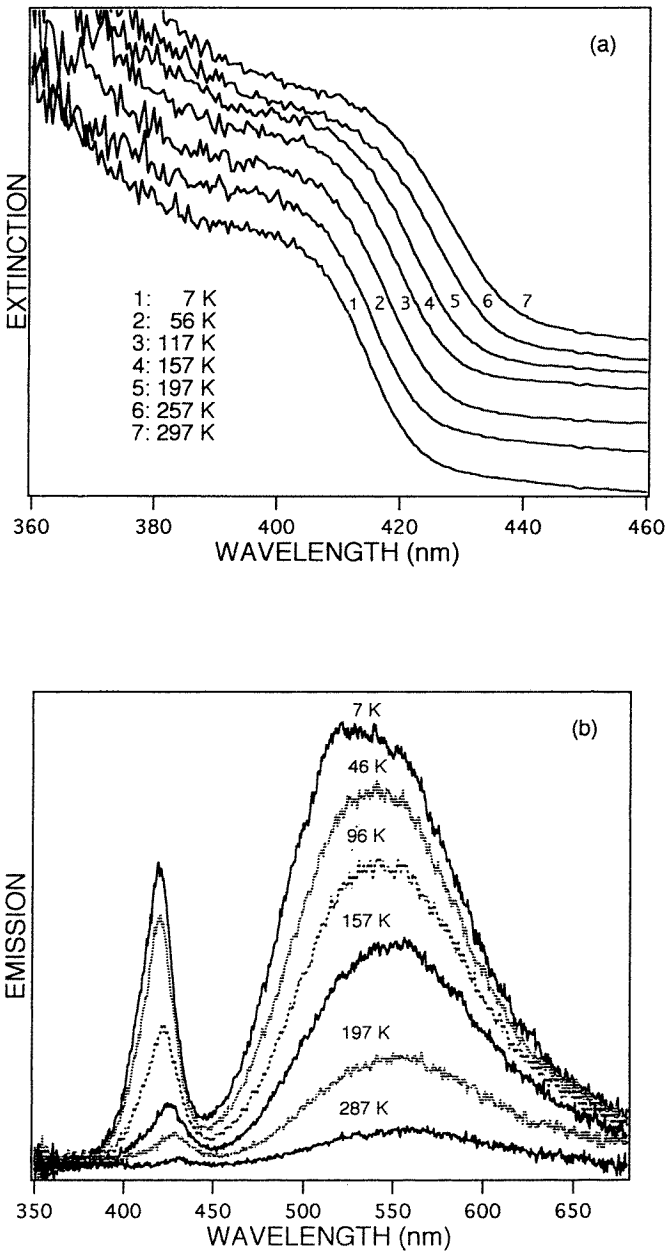

Figure 5. The extinction and photoluminescence spectra of ZnSe-doped Pyrex glass annealed for 910 minutes at various temperatures. (a) Extinction spectra. (b) Photoluminescence spectra.

(I) versus temperature (T) is expressed empirically as the exponential gap law:

$$I(T) = A/[B + C\exp(-\Delta E/kT)] \tag{2}$$

in which A and B are constants, C may be the transition probability of de-excitation by some nonradiative traps via thermal activation at high temperatures, and ΔE is the

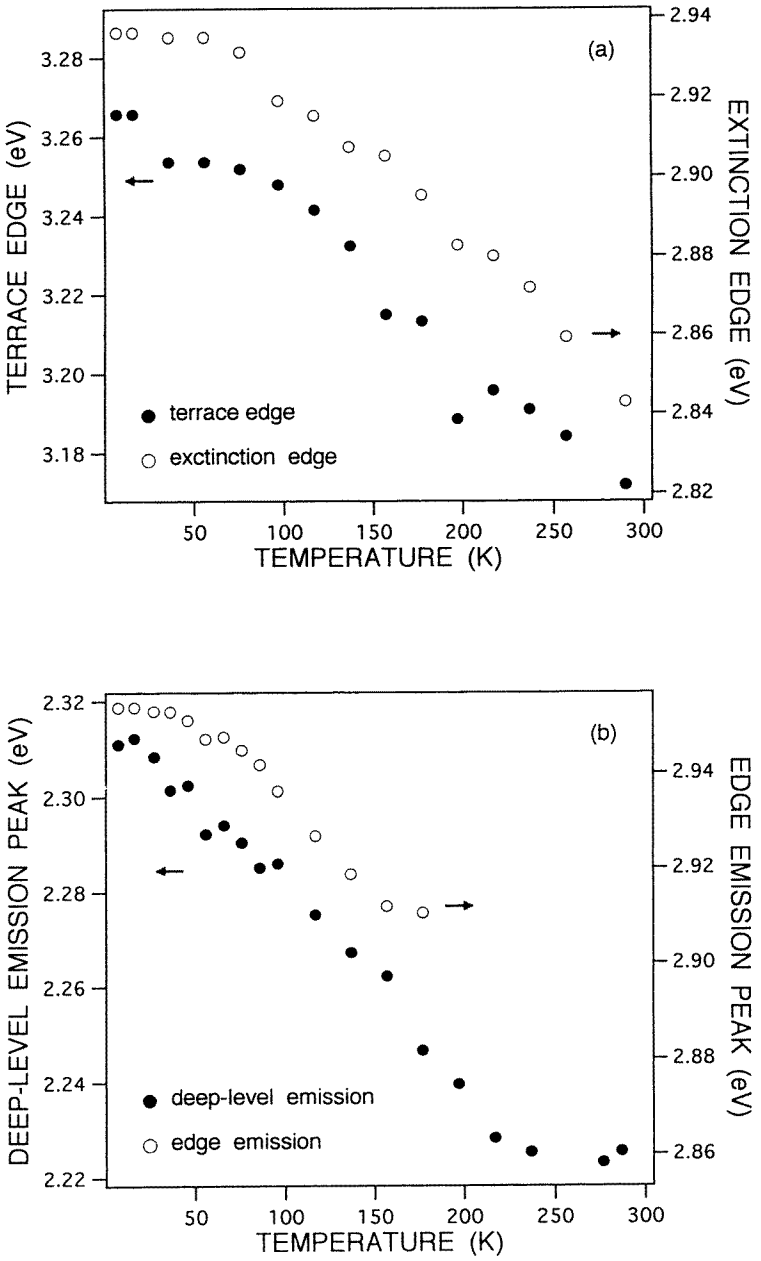

Figure 6. Temperature dependences of the extinction edge and terrace edge energies (a), and the edge emission peak and deep-level emission peak energies (b), of ZnSe-doped Pyrex glass heat treated for 910 minutes.

activation energy of the process. Solid curves were obtained by fitting the curves calculated from equation (2) so as to suit the data obtained mainly at high temperatures. The activation energies for the edge and deep-level emissions are about 210 cm^{-1} and about 320 cm^{-1}, respectively. These energies are close to the optical phonon energies (about

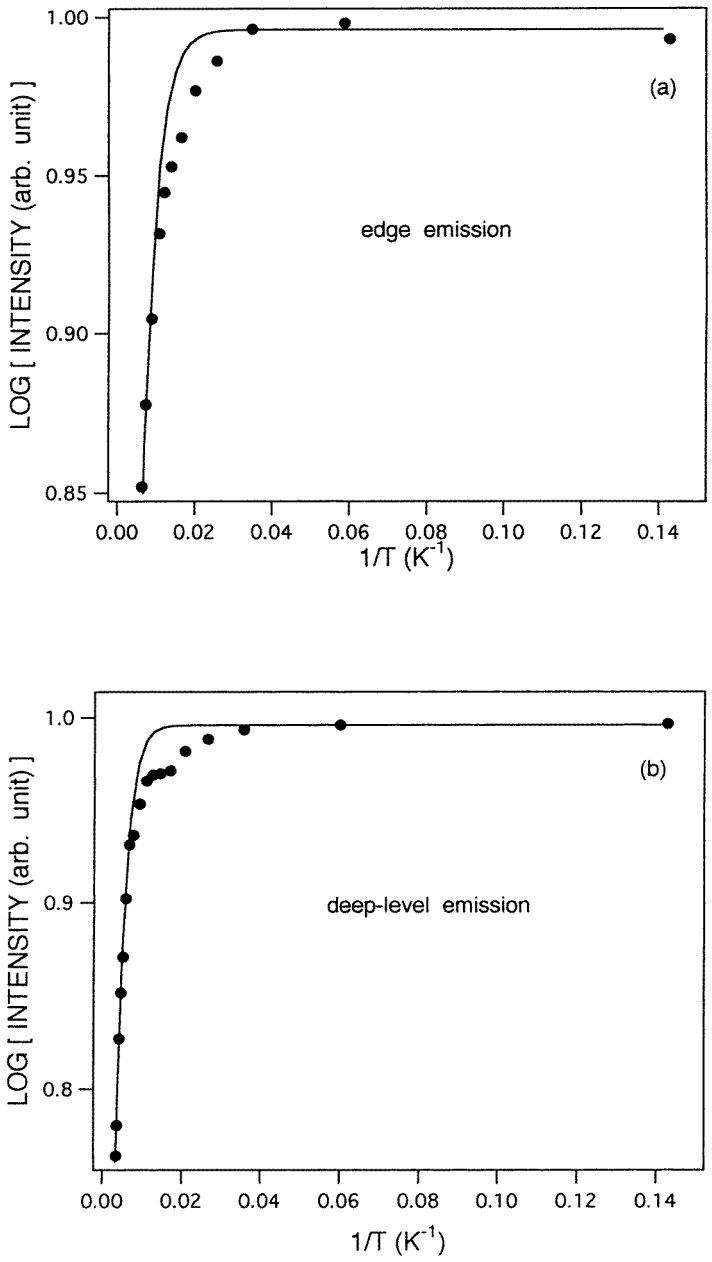

Figure 7. Temperature dependences of the edge and deep-level emission intensities of ZnSe-doped Pyrex glass heat treated for 910 minutes. (a) Edge emission. (b) Deep-level emission.

210 cm^{-1} and 250 cm^{-1}) for bulk ZnSe crystal. Using the adiabatic potential curves of free (carrier or exciton) and nonradiative trapped states which are intersecting, the trapping of carriers and excitons is explained as thermal fluctuation of the lattice system. The thermal fluctuation induces the electronic transition from the potential minimum of the free state to

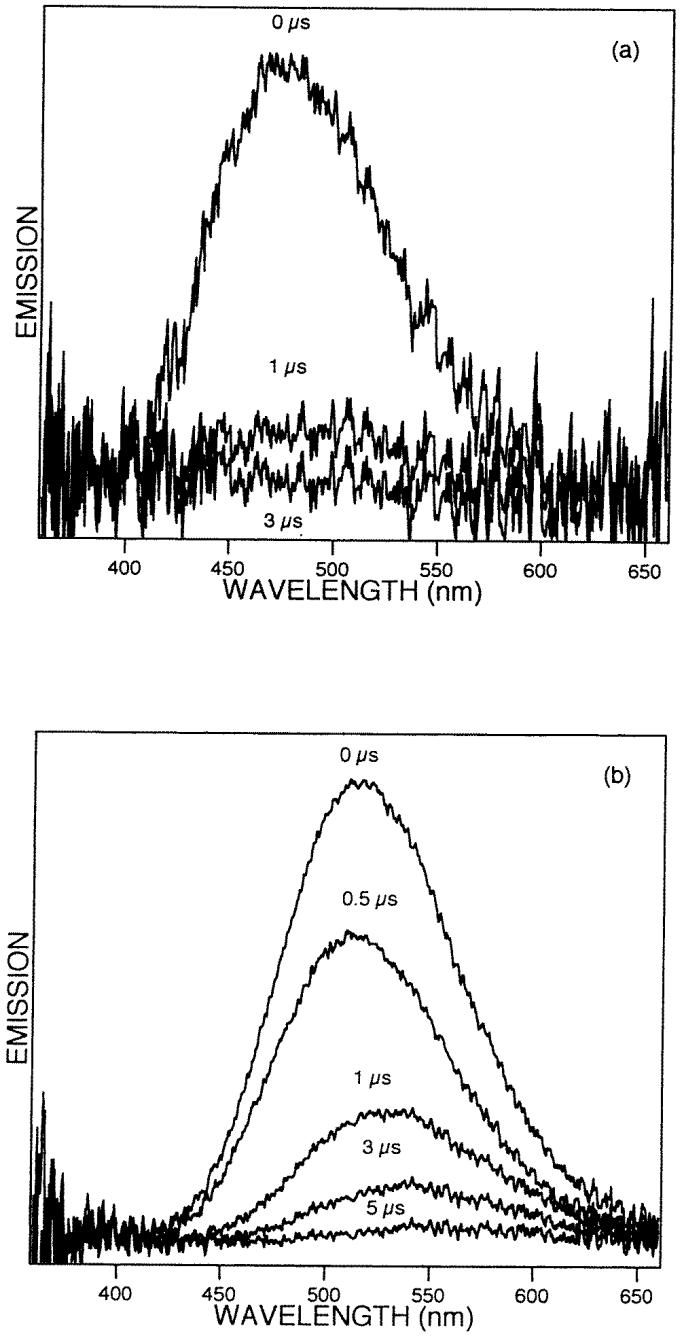

Figure 8. Time-resolved spectra of ZnSe-doped Pyrex glass heat treated for 35 minutes (a) and 910 minutes (b), at 8 K.

the nonradiative potential curve at their intersection. The difference between the energy at the minimum and that at the intersection may correspond to the activation energy observed.

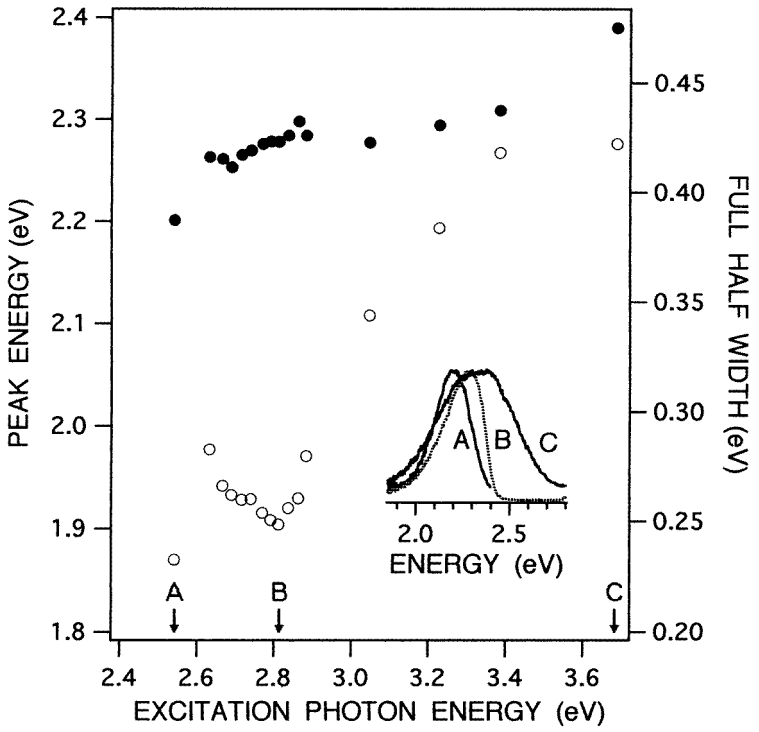

Figure 9. Excitation energy dependences of the intensity peak energy (solid circles) and full half-width (open circles) of the deep-level emission band of ZnSe-doped Pyrex glass at 7 K.

3.3. Time evolution and excitation photon energy dependence of the deep-level emission

Figures 8(a) and 8(b) show the time-resolved spectra of the specimens heat treated for 35 minutes and 910 minutes, respectively. In the figures, the numbers beside the spectra indicate the time elapsed after photoexcitation (i.e., delay time). The measurements were carried out at 8 K. Since, unfortunately, our measurement system has the inherent time delay of 85 ns, the edge emission with a short decay time ($\ll$ 85 ns) is not observed in the time-resolved measurements. As seen in these figures, the decay time of deep-level emission increases with increasing annealing time (i.e., crystallite size), and the emission band shifts to longer wavelength with increasing delay time. If we assume a uniform size distribution, the results may indicate that the broad deep-level emission band arises from many quasi-continuous luminescent electronic levels in each crystallite or strong electron–phonon interaction. In the former case, the spectrum should be time resolved as we observed, while, in the latter case, such a broad band is not time resolved, in such a microsecond region. Therefore, as long as we assume a uniform size of crystallites, it is concluded that the deep-level emission observed arises from many quasi-continuous luminescent electronic levels.

Incidentally, it is interesting to study whether the deep-level emission in microcrystals is affected by quantum confinement or not. Theoretically, the peak energy and width of an edge emission band increase with increasing incident photon energy (confinement energy), but those of the deep-level emission band in microcrystals are not fully clarified (Bawendi *et al* 1992, Brus 1994). Therefore, we measured the photoluminescence spectra by the size-

selective excitation method with a tunable UV laser. The peak energy (solid circles) and width (open circles) of the deep-level emission band for the specimen heat treated for 910 minutes are plotted as functions of excitation photon energy in figure 9. The measurements were carried out at 7 K. As seen in this figure, the observed peak energy and band width tend to decrease with decreasing incident photon energy. Above the extinction edge energy ($>$2.94 eV), these behaviours may arise mainly from size selectivity in photoexcitation, though the absorption (extinction) bands are not limited to a narrow wavelength region. If this is so, the quantized sublevel in each crystal is accompanied by a corresponding level giving the deep-level emission. The origin of the broadening on the higher-energy side may be due to the deterioration of size selectivity and due to the increased surface scattering of carriers or excitons in smaller crystallites. It is noted that we can observe also a weak broad emission band in the neighbourhood of 2 eV, even under excitation photon energy lower than the extinction edge energy. Such emission may arise mainly from the direct excitation of various luminescent impurity levels inside the energy gap. The width certainly shows a complicated behaviour below 2.8 eV, as shown in figure 9. In this figure, the spectra obtained under three different excitation energies, 3.68 eV (C), 2.81 eV (B) and 2.54 eV (A), are shown.

3.4. The origin of the deep-level emission

By comparing the spectra of the ZnSe-doped glass with those of ZnSe bulk crystal and of the nominally pure thick (bulk-like) ZnSe film, we discuss the origin of the deep-level emission band for microcrystals. The intense deep-level emission observed in ZnSe-doped glass is hardly observed in the ZnSe bulk crystal at room temperature and is characteristic of ZnSe-doped glass. Such deep-level emission may be due to some crystalline defects or impurities which came from the matrix glass during microcrystal growth.

First we refer to the ZnSe film data reported by Mohapatra *et al* (1988). The emission spectra observed in the film specimens consist of a sharp emission band near the absorption edge and a broad emission band below about 2 eV, similar to the case of our microcrystal specimens. Mohapatra *et al* assigned the broad-band emission (deep-level emission) to excess zinc vacancies V_{Zn}, by taking into account the selenium vacancies V_{Se} discussed in the previous section, and obtained a deep-level emission energy $E(\mathrm{DP})$ of 2.035 eV from the following relation:

$$E(\mathrm{DP}) = E_g - E(V_{Zn}) - E(V_{Se}) \tag{3}$$

where E_g, $E(V_{Zn})$ and $E(V_{Se})$ are 2.7 eV, 0.65 eV and 0.025 eV, respectively. Since such deep-level emission is prominent in film specimens which have a large ratio of surface area to volume, the deep-level emission may be enhanced in microcrystal specimens as observed in the present study.

Next, we discuss the impurity effects, since there is some possibility of contamination due to environmental sodium and boron atoms which are constituent elements of the Pyrex glass matrix. In the studies of ZnSe films, it is pointed out that sodium atoms act as shallow acceptors (Bouley *et al* 1975) and boron atoms may act as shallow donors. In this case, the shallow-donor–shallow-acceptor recombination cannot give any deep-level emission such as that we observed.

Additionally, it should be noted that the defect-induced (deep-level) emission becomes prominent in the film and microcrystal specimens. Comparing with bulk crystal, the ratios of surface area to volume in film and microcrystals increase with decreasing film thickness and crystallite size, respectively. Therefore, it may be natural to assume that such defects are

near the crystallite surfaces, though it is very difficult to determine whether the deep-level emission comes from the crystallite surface or from the interior of the crystallite. Moreover, it should be noted that, since matrix glass has a variety of atomic arrangements around the crystallite, there are various kinds of surface electronic state even in a crystallite, according to the respective surface sites.

4. Summary and remarks

Optical spectra of ZnSe microcrystals embedded in Pyrex glass have been measured for the first time. The microcrystals exhibit a shift of the optical absorption (extinction) edge due to the spatial confinement of carriers in three dimensions. Also, the photoluminescence spectra show a weak edge emission band at the respective absorption edges and an intense broad deep-level emission band at longer wavelength. The broad deep-level emission band may arise from various electronic states which are due to crystallite defects owing to nonstoichiometry. The excitation photon energy dependence indicates that the sublevels in the conduction and valence bands are accompanied by levels which give the deep-level emission.

However, for smaller microcrystals, the effects caused by the surroundings may have interfered more with the exciton and carrier confinement effects. Therefore, it is desirable to study the optical spectra of both free and embedded microcrystals for a given material. Very recently, we have developed a simple measurement method for free microcrystals using time-resolved and space-resolved spectroscopies applied to the vapour zone (Mochizuki and Ruppin 1993, Mochizuki and Nakata 1993, Mochizuki *et al* 1994) and the microcrystal beam (Mochizuki *et al* 1995) generated by thermal evaporation in a noble-gas stream. The results of an optical study on free ZnSe microcrystals will be reported in the near future.

References

Bawendi M G, Carroll P J, Wilson W L and Brus L E 1992 *J. Chem. Phys.* **96** 946
Borrelli N F, Hall D W, Holland H J and Smith D W 1987 *J. Appl. Phys.* **61** 5399
Bouley J C, Blanconnier P, Herman A, Ged P, Henoc P and Noblanc J P 1975 *J. Appl. Phys.* **46** 3549
Brus L E 1984 *J. Chem. Phys.* **80** 4403
——1986 *IEEE J. Quantum Electron.* **22** 1909
——1994 *Nanophase Materials* ed J C Hadjipanayis and R W Siegel (Netherlands: Kluwer–Academic) pp 433–48
Chestnoy N, Hull R and Brus L E 1986 *J. Chem. Phys.* **85** 2237
Efros Al L and Efros A L 1982 *Fiz. Tekh. Poluprov.* **16** 1209 (Engl. Transl. 1982 *Sov. Phys.–Semicond.* B **16** 772)
Kayanuma Y 1988 *Phys. Rev.* B **38** 9797
Lifshitz I M and Slezov V V 1958 *Zh. Eksp. Teor. Fiz.* **35** 479
Mochizuki S and Nakata H 1993 *Phys. Lett.* **183A** 390
Mochizuki S, Nakata H and Asanuma M 1996 *Proc. ISSPIC7; Surf. Rev. Lett.* **3** 523
Mochizuki S, Nakata H and Ruppin R 1994 *J. Phys.: Condens. Matter* **6** 1269
Mochizuki S and Ruppin R 1993 *J. Phys.: Condens. Matter* **5** 135
Mohapatra S K, Haugen G A, Cheng H, Potts J E and DePuydt J M 1988 *SPIE* **944** 56
Skromme B J, Shibli S M, de Miguel J L and Tamargo M C 1989 *J. Appl. Phys.* **65** 3999
Warnock J and Awschalom D D 1985 *Phys. Rev.* B **32** 5529